34th Annual International Conference of the IEEE EMBS
San Diego, California USA, 28 August - 1 September, 2012

On localizing a Capsule Endoscope using Magnetic Sensors

Babak Moussakhani, Tor Ramstad, John T. Flåm and Ilangko Balasingham*

Abstract

In this work, localizing a capsule endoscope within the gastrointestinal tract is addressed. It is assumed that the capsule is equipped with a magnet, and that a magnetic sensor network measures the flux from this magnet. We assume no prior knowledge on the source location, and that the measurements collected by the sensors are corrupted by thermal Gaussian noise only. Under these assumptions, we focus on determining the Cramer-Rao Lower Bound (CRLB) for the location of the endoscope. Thus, we are not studying specific estimators, but rather the theoretical performance of an optimal one. It is demonstrated that the CRLB is a function of the distance and angle between the sensor network and the magnet. By studying the CRLB with respect to different sensor array constellations, we are able to indicate favorable constellations.

1. INTRODUCTION

When Given Imaging introduced the Capsule Endoscope in 2000, it revolutionized the gastrointestinal imaging field (GI). From the beginning it was clear that accurate localization was indispensable - pictures taken by the endoscope are obviously more valuable if they can be associated with precise locations. To tackle this challenge mainly two approaches have been proposed: (i) Received Signal Strength (RSS)-based methods and (ii) magnet-based methods. In RSS-based methods the power readings from the sensors are used to locate the endoscope, and the Pillcam from Given Imaging utilizes this technique. However, the achievable accuracy is shown to be no less than 3 cm [1], and it is even worse for large parts of the trajectory. In order to improve the performance, ultra wideband signals have been proposed [2]. However, spatially correlated shadowing limits the precision for RSS-based methods and keeps the achievable accuracy in the order of cm. Magnet-based localization, on the other hand, has proven to reach precisions in the order of mm [3, 4, 5]. The main reason is that these methods see a much more predictable channel, than the RSS-based counterpart, because human tissues have very similar magnetic permeability to air.

Magnet-based localization methods have so far mainly been studied for quite specific scenarios and setups [3, 4, 5]. As far as we know, there exists no studies that explain the general parameters that influence the localization accuracy. This paper provides such a contribution by deriving the Cramer-Rao Lower Bound (CRLB) on the localization and orientation of the endoscope. The CRLB is a lower bound on the variance of any unbiased estimator. In our setup, the CRLB becomes a function of the orientation and position of the magnet relative to the sensors. It can therefore be used, not only to determine the best expected performance by any sensor network, but also to derive good sensor network constellations.

2. System model and CRLB

It is assumed that the Capsule Endoscope (CE) includes a cylindrical magnet with length l and cross section (area of the cylinder base) s. The magnet is assumed to be magnetized along the main axis of the cylinder. The magnetic flux density produced by the magnet is observed by a magnetic sensor network. No specific assumption is made on the magnetic sensors except that their measurement noise is assumed to be independent and Gaussian. These assumptions enable us to reproduce the results in [3, 4], and to make comparisons.

2.1. Observation Model

The magnet is associated with a magnetization vector with amplitude $m_0 \geq 0$ (Amp/meter), and orientation $\mathbf{h_0} = [m,k,p]^T$, $\|\mathbf{h_0}\|^2 = m^2 + k^2 + p^2 = 1$, in Cartesian coordinates. Throughout the paper we will assume that

**This work was supported by the Research Council of Norway (RCN) NFR under Melody Project. B. Moussakhani, T.Ramstad and J.T. Flåm are with Department of Electronics and Telecommunications, NTNU, N-7491 Trondheim, Norway. Emails: [babak,ramstad,flam] at iet.ntnu.no. I. Balasingham is with Intervention Center, Oslo University Hospital, N-0027 Oslo, Norway and The istitute of clinical medicine at University of Oslo N-0318 Oslo, Norway. Email: ilangkob at medisin.uio.no

the magnet is located at $[a,b,c]^T$, where a,b,c can vary. The magnetic flux vector $\mathbf{b_n}$ seen by sensor n, located at $[x_n,y_n,z_n]^T$, can then be calculated as [6]:

$$\mathbf{b_n} = b_T \left(\frac{3(\mathbf{h_0}^T \mathbf{d_n})\mathbf{d_n}}{\|\mathbf{d_n}\|^5} - \frac{\mathbf{h_0}}{\|\mathbf{d_n}\|^3} \right) \quad (n = 1,2,\cdots N) \quad (1)$$

where $b_T = (\mu_r \mu_0 slm_0)/(4\pi)$, μ_r is the relative permeability of the medium and $\mu_0 = 4\pi \times 10^{-7}$ is the magnetic permeability of the air. In (1), N is the number of spatial points (sensors) in the array, $\mathbf{d_n} = [x_n - a, y_n - b, z_n - c]^T$ is the vector from the sensor location to the magnet location, and $\|\mathbf{d_n}\| = \sqrt{\mathbf{d_n}^T \mathbf{d_n}}$ is its Euclidean norm. Figure 1 portrays an example where the flux of the magnet is measured by a 2D sensor array. As depicted in Figure 1 the magnet orientation can be represented using spherical coordinates, where the two angles are θ, φ. It is assumed that the thermal noise is the only source of errors, and this noise is considered to be Gaussian. All sensors in the array are identical and able to measure the magnetic flux along all three directions. Thus the fusion center has access to $3 \times N$ measurements. The observation vector can be written as

$$\mathbf{p} = \begin{bmatrix} \mathbf{p_1} \\ \mathbf{p_2} \\ \vdots \\ \mathbf{p_N} \end{bmatrix} = \begin{bmatrix} \mathbf{b_1} \\ \mathbf{b_2} \\ \vdots \\ \mathbf{b_N} \end{bmatrix} + \mathbf{w}, \quad (2)$$

where the noise, $\mathbf{w} \sim \mathcal{N}(\mathbf{0}, \sigma^2 \mathbf{I})$, is the only random contribution. In this paper σ is set to be 1.2×10^{-8} which is the magnetic resolution specified by the manufacture for (Honeywell HMC1043) magnetic sensors. The reason for such an assumption is to consider a scenario close to the implementation in [3], and to allow comparisons.

2.2. Lower Bound on Localization Accuracy

The likelihood function, which depends on 6 deterministic unknown parameters, $\zeta = [a,b,c,m,k,p]^T$, can be written as:

$$f_\zeta(\mathbf{p};\zeta) = \prod_{n=1}^{N} \frac{1}{\sqrt{2\pi}\sigma} e^{-\frac{1}{2\sigma^2}\|\mathbf{p_n} - \mathbf{b_n}\|^2}. \quad (3)$$

The dependency on ζ is via the term $\mathbf{p_n} - \mathbf{b_n}$. According to the definition, the (i,j)-th element of Fisher Information Matrix (FIM) for the vector ζ can be found as

$$\mathbf{I}_{ij} = \mathbf{E}[-\frac{\partial^2}{\partial \zeta_i \partial \zeta_j} \ln f_\zeta(\mathbf{P};\zeta)]. \quad (4)$$

The individual elements of the FIM are given in equations (9)-(14) of the Appendix. It is convenient to study

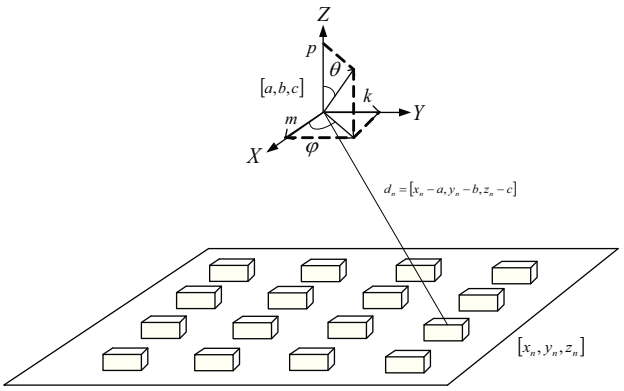

Figure 1. 2D sensor array with equally spaced sensors around the origin.

the CRLB in terms of the two angles in spherical coordinates, (θ,φ), rather than the three parameters in Cartesian coordinates (m,k,p). Therefore we express the CRLB for the vector $\eta = (a,b,c,\theta,\varphi)$ based on the derived FIM elements for ζ. (θ,φ) are related to (m,k,p) by:

$$\begin{aligned} \theta &= \sin^{-1}\left(\frac{p}{\sqrt{m^2+k^2+p^2}}\right) = \sin^{-1}(p) \quad (5) \\ \varphi &= \cos^{-1}\left(\frac{m}{\sqrt{m^2+k^2}}\right). \end{aligned}$$

Hence, the Jakobian matrix for calculating CRLB for $(\theta,\varphi)^T$ from (m,k,p) can be written as:

$$\mathbf{K} = \begin{bmatrix} 0 & 0 & \frac{-1}{\sqrt{1-p^2}} \\ \frac{-k}{m^2+k^2} & \frac{-m}{m^2+k^2} & 0 \end{bmatrix}. \quad (6)$$

Therefore, the CRLB for η based on the chain rule [7] is calculated as:

$$\begin{aligned} CRLB_\eta &= \mathbf{H}\mathbf{I}_\zeta^{-1}\mathbf{H}^T \quad (7) \\ \mathbf{H} &= \begin{bmatrix} \mathbf{I}_{3\times3} & \mathbf{0}_{3\times3} \\ \mathbf{0}_{2\times3} & \mathbf{K} \end{bmatrix} \end{aligned}$$

Inspecting (7) and (9)-(13) it can be determined that the CRLB is a function of two parameters: first the distance between the magnet and the sensors array and the second the relative magnet orientation. Clearly, increasing the distance between the magnet and the sensor array increases the CRLB. On the other hand it is less clear how the CRLB reacts to the orientation changes.

3. Observations

We now investigate the CRLB under different scenarios in order to provide a better understanding of the best achievable localization performance, and to suggest possible constellations for the sensor array.

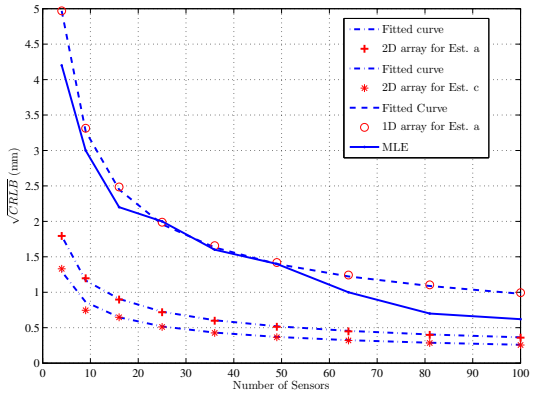

Figure 2. $\sqrt{\text{CRLB}}$ for 2D array in estimating a and c and 1D array for estimating a.

3.1. Increasing the Number of Sensors

Consider a scenario similar to Figure 1 where the sensor nodes are distributed uniformly within a 0.5×0.5 square of the (x,y)-plane. The center of the square coincides with the origin. The magnet is located at $[0,0,0.25]^T$, and all dimensions are in meters. First we study the effect of increased sensor density (the number of sensors in the square is increased). Then, we repeat the same experiment, but place all sensors along the x-axis (from -0.25 to 0.25). The magnet orientation is kept along the z-axis, $\mathbf{h_0} = [0,0,1]^T$, for both scenarios.

Figure 2 shows the square root of the CRLB for estimators of a and c (the first and third coordinate of the endoscope). Note that because the sensor constellation in the (x,y)-plane is symmetric around the origin, the CRLB for b will be the same as for a. From the plot, it is clear that spreading sensors along two dimensions lowers the CRLB. It is known, that for parameter estimation in white noise, the CRLB declines with $1/N$, where N is the number of observations [7]. Therefore we fit a curve with slope $1/\sqrt{N}$ to both scenarios. This matches closely the $\sqrt{\text{CRLB}}$ curves for both cases, which provides a simple indication that our CRLB calculations are correct. Note that the CRLB for estimation of c is lower than CRLB for estimation of a. This is in line with results in [3, 4], and happens because the magnet is aligned along z-axis. In addition to CRLB plots, Figure 2 also depicts the mean error norm of the Maximum Likelihood Estimator (MLE) for and increasing number of sensors. The MLE is implemented to estimate a using a 2 dimensional sensor array, and its performance curve should therefore be compared to the bound labeled as *2D array for Est. a*. It can be seen that the gap between these curves decreases as the number of sensors increases. Since MLE is asymptotically efficient, this is expected. Observe also that the performance of the MLE is very close to what was reported in [3, 4]. There, the accuracy for 16 sensors was approximately 2 mm, which is similar to what we obtain.

3.2. Increasing the Distance

In order to investigate the CRLB under increasing distance to the sensor array, we assume the magnet is located at $(0,0,c)$ and vary c from 10 to 100 cm. As before, we study the CRLB for estimation of a and c. The elements in FIM (9)-(13) are inversely proportional to a polynomial function of distance with the least degree of 6. Therefore, $\sqrt{\text{CRLB}}$ is described by a polynomial function of distance with minimum degree of 3. Figure 3 portrays $\sqrt{\text{CRLB}}$ as a function of distance. Comparing the curves, the CRLB for estimating c is lower than for estimating a, as long as the magnet is close to the plane. However, after a point the trend is reversed. The reason is that after this point, on the average, the sensors are closer to the magnet in x-direction than in z-direction. To provide a general picture of how the CRLB increases with increasing distance, two polynomials proportional to c^3 and c^5, respectively, are also plotted. It can bee seen that $\sqrt{\text{CRLB}}$ is located in between these two polynomials. For the small to moderate distances the c^3 curve is a very good fit for $\sqrt{\text{CRLB}}$, while it deviates from $\sqrt{\text{CRLB}}$ as the distance grows. For larger distances $\sqrt{\text{CRLB}}$ becomes closer to c^5. This result is in line with the results in [4], where the authors concluded that the localization error is proportional to the 3rd power of the distance. However they did not continue the experiment for larger distances. Therefore, in general, the localization error does not follow such a simple rule of thumb. This could be of importance, for example, if the sensor network cannot be mounted on the patient, but has to be further away.

3.3. Change in the Orientation

In order to study the orientation effect on the CRLB, we evaluate the CRLB for estimation of a,b,c for a scenario where the magnet rotates 90° toward the y axis. In other words orientation changes gradually from $\mathbf{h_0} = [0,0,1]^T$ to $\mathbf{h_0} = [0,1,0]^T$. Figure 4 shows the results for such a scenario. It is clear that such a rotation, results in a smaller CRLB for estimating a and b, and a larger for estimating c. Such a result is due to the fact that the flux of a magnet in the far field is maximum along its magnetization vector [6].

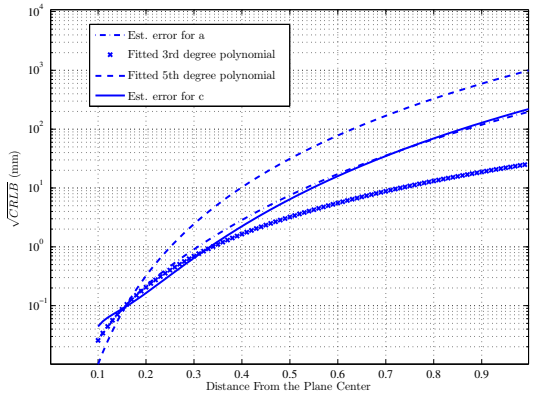

Figure 3. $\sqrt{\text{CRLB}}$ for estimating a and c, as a function of the distance c from the origin together with fitted curves proportional to c^3 and c^5.

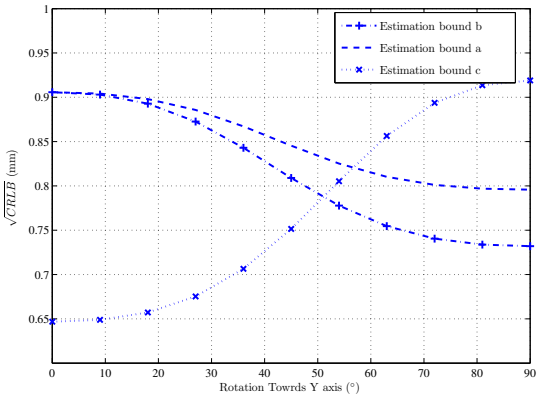

Figure 4. $\sqrt{\text{CRLB}}$ for estimation of a, b, c for a rotating magnet.

3.4. Two Parallel Planes

In order to observe the effect of the sensor network constellation on the CRLB, two different setups are studied as follows. Two planes are deployed with 16 sensors similar to Figure 1. In the first setup (Case 1), the two planes are located parallel to (x,y)- plane at $z = 0$ and $z = 0.6$ m while in the second setup (Case 2), both planes are located at $z = 0$, i.e. two magnetic sensors are placed at each position. The magnet is considered to be moving on a straight line from $(-0.3,-0.3,0.3)$ to $(0.3,0.3,0.3)$. Two orientations are considered: $\mathbf{h_0} = [0,0,1]^T$ and $\mathbf{h_0} = \frac{1}{\sqrt{3}}[1,1,1]^T$. Figure 5 shows $\sqrt{\text{CRLB}}$ for estimating b for the two setups together with $\sqrt{\text{CRLB}}$ when using only one plane with 16 sensors. The results from the latter setup are close to measurement results in [4, 3], and repeated here to emphasize that the theoretical bounds are close to practical results. As expected, placing two sensors in the same physical location decreases the CRLB compared to using only one. The reason is that the former provides better noise averaging. However, a major improvement, for both orientations, is obtained when two planes are placed in two different locations on the z-axis. It should be emphasized that the two distance matrices, which contain the distances between the magnet and all of the sensors in a plane, are identical. Therefore the magnitude of the fields measured by sensors in both planes are also identical. However, the direction of the fields are different. Thus designing sensor constellations such that they experience *flux diversity*, seems to be a good principle.

Note also from Figure 5, that the curve for Case 2 is not symmetric around the origin when $\mathbf{h_0} = \frac{1}{\sqrt{3}}[1,1,1]^T$. This symmetry breaking happens because the magnet is not orthogonal to the plane. However, when using two planes, as in Case 1, a symmetric and decreased CRLB results. Thus, in terms of network constellation design, improved performance may be achieved by distributing sensors to different planes, which in practice means 3D sensor networks. The design principle may be summarized by two conflicting criteria: (i) to place the sensors as far as possible from each other and (ii) as closely as possible to the magnet.

4. Comparison to RSS-based localization

Since the introduction of the capsule endoscopy, RSS-based localization has been the default technique. It is claimed to reach 3 cm precision [1], but this accuracy varies and can change for different people and different parts of the GI track. Using ultra wideband signals has proven to increase the accuracy [2] and to make the localization accuracy less variable for all parts of the digestive track. However the spatial correlation in the shadowing puts a limit to achievable accuracy which is independent of sensor numbers in the network i.e. increasing number of sensors does not improve the estimation accuracy. In contrast, magnet-based localization is much less affected by the medium due to an almost constant magnetic permeability of human tissues $\mu_r = 1$ throughout the body. As demonstrated in this paper, magnet-based localization has the potential to reach millimeter accuracy for distances below 30 cm and it is also expected to maintain such an accuracy throughout the digestive track [3]. In addition, magnet-based localization enables estimation of the orientation of the magnet which can be used for controlling the endoscope

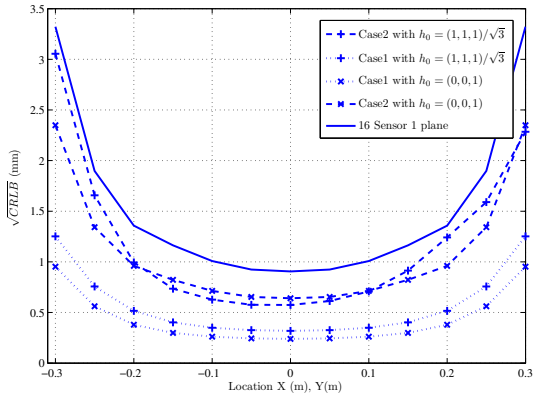

Figure 5. $\sqrt{\text{CRLB}}$ for estimating b when the sensors are placed on two parallel planes (Case 1) or in one plane (Case 2).

movements.

5. Conclusion

In this paper, the CRLB for the position of a magnetic sensor network has been presented. The results are consistent with previous research and measurements. The CRLB is a function of the distance and orientation between the magnet and the sensors. The effect of different network constellations has been investigated and we find that placing sensors cleverly increases the localization accuracy. Comparing the results to other methods it is concluded that using magnet-based localization of a capsule endoscope has great potential in terms of accuracy, and it also enables estimating the orientation of the capsule endoscope.

6. Appendix

Taking the derivative and mean from (4) results:

$$I_{jl} = \frac{1}{\sigma^2}\sum_{n=1}^{N} i_{jl}^n, \tag{8}$$

$$i_{jl}^n = \frac{\partial B_{nx}}{\partial \zeta_j}\frac{\partial B_{nx}}{\partial \zeta_l} + \frac{\partial B_{ny}}{\partial \zeta_j}\frac{\partial B_{ny}}{\partial \zeta_l} + \frac{\partial B_{nz}}{\partial \zeta_j}\frac{\partial B_{nz}}{\partial \zeta_l}, \tag{9}$$

so elements in FIM with respect to ζ vector can be calculated as follows:

$$i_{aa} = \frac{(q+6mx)^2+9(my+kx)^2+9(mz+px)^2}{\|\mathbf{d_n}\|^{10}} + \frac{25q^2x^2(\frac{36}{25}x^2+y^2+z^2)}{\|\mathbf{d_n}\|^{14}} - \frac{6qx(5y(my+kx)+5z(mz+px)+2(q+6mx)x)}{\|\mathbf{d_n}\|^{12}}, \tag{10}$$

$$i_{ab} = \frac{9(mz+px)+3(my+kx)(3q-pz)}{\|\mathbf{d_n}\|^{10}} + \frac{30q^2xy(x^2+y^2+\frac{25}{30}z^2)}{\|\mathbf{d_n}\|^{14}} - \frac{18q(my+kx)(x^2+y^2)+5qxy(4q-6pz)+15qz(x(kz+py)+y(mx+pz))}{\|\mathbf{d_n}\|^{12}}, \tag{11}$$

$$i_{am} = \frac{q+6mx}{\|\mathbf{d_n}\|^{8}} - \frac{3x^2(3q+6mx)+9xy(my+kx)+9xz(mz+px)}{\|\mathbf{d_n}\|^{10}} + \frac{15qx^2(\frac{18}{15}x^2+y^2+z^2)}{\|\mathbf{d_n}\|^{12}}, \tag{12}$$

$$i_{ak} = \frac{3(my+kx)}{\|\mathbf{d_n}\|^{8}} - \frac{xy(8q+18mx)+9y^2(my+kx)+9z^2(mz+px)}{\|\mathbf{d_n}\|^{10}} + \frac{15qxy(\frac{18}{15}x^2+y^2+z^2)}{\|\mathbf{d_n}\|^{12}}, \tag{13}$$

$$i_{mm} = \frac{3x}{\|\mathbf{d_n}\|^{8}} + \frac{1}{\|\mathbf{d_n}\|^{6}} \quad i_{mk} = \frac{3xy}{\|\mathbf{d_n}\|^{8}}, \tag{14}$$

where,

$$\begin{aligned} x &= x_n - a, \;\; y = y_n - b, \;\; z = z_n - c, \\ q &= mx + ky + pz. \end{aligned} \tag{15}$$

The other diagnonal elements of FIM can be calculated similar to i_{aa}, i_{mm} and other off-diagonal elements are calculated based on $i_{ab}, i_{am}, i_{ak}, i_{mk}$.

References

[1] G. Iddan, G. Meron, A. Glukhovsky, and P. Swain, "Wireless capsule endoscopy," *Nature*, vol. 405, no. 6785, pp. 417–417, May 2000.

[2] B. Moussakhani, J. Flå m, S. Stø a, I. Balasingham, and T. Ramstad, "On localisation accuracy inside the human abdomen region," *IET Wireless Sensor Systems Journal*, vol. 2, no. 1, p. 9, 2012.

[3] C. Hu, M. Li, S. Song, W. Yang, R. Zhang, and M. Q. Meng, "A cubic 3-Axis magnetic sensor array for wirelessly tracking magnet position and orientation," *IEEE Sensors Journal*, vol. 10, no. 5, pp. 903–913, May 2010.

[4] Schlageter, "Tracking system with five degrees of freedom using a 2D-array of hall sensors and a permanent magnet," *Sensors and Actuators A: Physical*, vol. 92, no. 1-3, pp. 37–42, 2001.

[5] C. Hu, M. Q. Meng, and M. Mandal, "A linear algorithm for tracing magnet position and orientation by using Three-Axis magnetic sensors," *IEEE Transactions on Magnetics*, vol. 43, no. 12, pp. 4096–4101, Dec. 2007.

[6] D. K. Cheng, *Field and Wave Electromagnetics*, 2nd ed. Addison-Wesley, Jan. 1989.

[7] S. M. Kay, *Fundamentals Of Statistical Signal Processing*. Addison Wesley Longman, Mar. 2001.